

Continuum modeling of cohesive and compressible granular matter

Lars Blatny^{1,2,3,*}, Nico Gray⁴, and Johan Gaume^{1,2,3},

¹Institute for Geotechnical Engineering, ETH Zürich, CH-8093 Zürich, Switzerland

²WSL Institute for Snow and Avalanche Research SLF, CH-7260 Davos Dorf, Switzerland

³Climate Change, Extremes, and Natural Hazards in Alpine Regions Research Center CERC, CH-7260 Davos Dorf, Switzerland

⁴Department of Mathematics and Manchester Centre for Nonlinear Dynamics, University of Manchester, Manchester M13 9PL, UK

Abstract.

In this contribution, we discuss the ability of elasto-viscoplastic constitutive models in capturing the diverse behavior of granular media as both solids and liquids. In particular, we showcase the recently developed MCC- $\mu(I)$ -rheology [1], which combines the Modified Cam-Clay (MCC) model for granular solids with the $\mu(I)$ -rheology for granular liquids, creating a “best-of-both-worlds” model for describing granular solids and liquids in a single framework. This model is demonstrated on various problems, including granular collapse tests as well as full-scale avalanche modeling.

1 Introduction

Continuum modeling of granular media is a challenging task, especially since such media can show characteristics of both solids and fluids under different conditions. In particular, a complete mechanical model should account for, e.g., elastic forces, shear band formation, varying internal friction and varying bulk density depending on the rate of the flow. In addition, some systems may also display a varying degree of cohesion due to attractive forces between the grains. Recently, the topic of cohesion in granular flows has gained significant interest in the granular flow communities. This includes the alpine hazard communities as, e.g., an increasing proportion of wet and cohesive snow avalanches in many areas is expected as a result of climate change. Snow is also an example of a granular material which can undergo large density variations.

As an alternative to the typical fluid mechanics approach for granular flows, we propose here to rely on an elasto-viscoplastic theory. Such a framework permits the direct treatment of dilation and compaction through defining appropriate combinations of plastic flow rules and hardening laws. Additionally, cohesion is easy to account for in elastoplastic models by carefully choosing the yield surface. In particular, we will in Sec. 4 consider the elastoplastic theory of Critical State Soil Mechanics (CSSM) [2], especially the Modified Cam-Clay (MCC) model [3], and its combination with the $\mu(I)$ -rheology [4, 5] which has become well-established to describe dense granular flow. The general idea of combining CSSM with the $\mu(I)$ -rheology was conceived by [6, 7] showing that compressibility introduced in the sense of CSSM can provide well-posedness to the $\mu(I)$ -rheology for all inertial numbers.

The elastoplastic approach to model both the solid and liquid behavior of granular media requires an appropriate numerical solver. For this reason, we consider the Material Point Method (MPM) due to the following advantages: 1) It does not suffer from mesh-distortion issues under extreme deformations or flow, 2) no special treatment of free-surface is needed and 3) complex terrains are easily specified and disconnection of the material from such boundaries are handled naturally. In the context of granular flows, to the best of our knowledge MPM was first used by [8] relying on a simple (cohesionless) Drucker-Prager yield surface. Later, [9] extended this to include the $\mu(I)$ -rheology. The models presented in this short paper may be regarded as a further extension to these pioneering works.

The numerical scheme of MPM is first presented in more detail, followed by an overview of elasto-viscoplastic theory. Next, the MCC- $\mu(I)$ -rheology model is introduced followed by examples of 3D simulations of granular collapse and flow.

2 The Material Point Method (MPM)

Typically credited to [10], MPM relies on a discretization of its domain by Lagrangian material points, each of which has a certain mass m_p , volume V_p , velocity \mathbf{v}_p , deformation gradient \mathbf{F}_p and other properties necessary to describe the material. In addition, an Eulerian grid is adopted to solve the momentum equation in a FEM-like manner. Neglecting the boundary term, an explicit temporal and spatial discretization of the weak form of the momentum conservation equation can be written on the Eulerian grid nodes i for each time step n of size Δt as

$$\frac{m_i^n \mathbf{v}_i^{n+1} - m_i^n \mathbf{v}_i^n}{\Delta t} = - \sum_p V_p \sigma_c(\boldsymbol{\varepsilon}_p^{E,n}) \nabla N_i(\mathbf{x}_p^n) + m_i^n \mathbf{g} \quad (1)$$

*e-mail: lars.blatny@slf.ch

where \mathbf{g} specifies gravity, N_i is an interpolation function and the nodal mass is $m_i^n = \sum_p m_p N_i(\mathbf{x}_p^n)$. Boundary conditions are applied directly to the updated grid velocities, promoting either no-slip or frictional slip with an imposed Coulomb friction. As m_p remains constant in time, mass conservation is automatically fulfilled. The (elasto-viscoplastic) constitutive law defining the relation $\boldsymbol{\sigma}_c(\boldsymbol{\varepsilon}^E)$ between the Cauchy stress $\boldsymbol{\sigma}_c$ and the (elastic part of the) strain measure $\boldsymbol{\varepsilon}^E$ is discussed in the next section.

Earlier criticism of MPM questioned cell-crossing instabilities and excessive numerical dissipation. The MPM community has in the last years addressed these issues by using B-spline interpolation functions [11] and by employing affine transfer schemes such APIC [12] and later AFLIP [13] to reduce dissipation.

3 Elasto-viscoplastic modeling

We start by specifying the elastic relation between the stress and the deformation. As we will be dealing with potentially large deformation, we avoid small strain assumptions and consider the multiplicative decomposition of the deformation gradient $\mathbf{F} = \mathbf{F}^E \mathbf{F}^P$ into its elastic and plastic part. The elastic deformation is in this work chosen to be determined by Hencky's model which has some very attractive properties as well as facilitating a relatively simple solution procedure. The reader is referred to, in particular, [14] for further details. In this isotropic and hyperelastic model, the Kirchhoff stress $\boldsymbol{\sigma} = \det(\mathbf{F})\boldsymbol{\sigma}_c$ is related to the (elastic part of the) Hencky strain $\boldsymbol{\varepsilon}^E$ through

$$\boldsymbol{\sigma} = \lambda(\text{tr } \boldsymbol{\varepsilon}^E)\mathbf{I} + 2G\boldsymbol{\varepsilon}^E \quad (2)$$

where \mathbf{I} denotes the second-order identity tensor, and λ and G are the two Lamé parameters which may be directly related to Young's modulus E and Poisson's ratio ν .

The onset of plastic deformations is characterized by a yield surface in stress space. With the velocity gradient $\mathbf{l} = \nabla \mathbf{v}$ being additively decomposed into an elastic and plastic part, $\mathbf{l}^E + \mathbf{l}^P$, a flow rule defines its plastic part to be given by $\mathbf{l}^P = \dot{\gamma} \frac{\mathbf{r}}{\|\mathbf{r}\|_F}$ where $\mathbf{r} = \mathbf{r}(\boldsymbol{\sigma})$ is a symmetric tensor and $\dot{\gamma}$ is the equivalent plastic strain rate. We assume in the following that the yield surface and flow rule defined through \mathbf{r} depend only on the two stress invariants $p = -\text{tr}(\boldsymbol{\sigma})/n_{\text{dim}}$ and $q = \sqrt{1/2 \boldsymbol{\tau} : \boldsymbol{\tau}}$ where $n_{\text{dim}} = 2$ or 3 denotes the number of spatial dimensions and $\boldsymbol{\tau}$ is the deviatoric Kirchhoff stress tensor. As such, a yield surface in the space of (p, q) can be defined as $q = q_y(p)$. Following the overstress approach of Perzyna [15], we can impose the plastic strain rate through

$$\dot{\gamma} = \begin{cases} 0, & \text{if } q \leq q_y(p) \\ \frac{1}{\eta} (q - q_y(p))^{1/s}, & \text{otherwise} \end{cases} \quad (3)$$

where η and s are viscous parameters. In particular, if $s = 1$, η represents a viscosity. In this case, and if q_y is considered a constant yield stress, the model reduces to a Bingham model for the plastic deformation.

The stress and strain states can be solved following the "elastic predictor – plastic corrector" operator splitting scheme of [16] in a finite strain framework.

4 The MCC- $\mu(I)$ -rheology model

While we can formulate and present this model in the overstress approach described in the previous section (see [1] for details), we take here a more straightforward approach.

We consider the yield surface given by the (cohesive) MCC model as defined in [17] as

$$q_y(p) = \mu \sqrt{(p + \beta p_c)(p_c - p)} \quad (4)$$

where $p_c \geq 0$ represents an isotropic compressive strength, $\beta \geq 0$ is a dimensionless measure of cohesion and $\mu > 0$ defines the slope of the Critical State Line (CSL) along which all critical states exist. This yield surface is sketched in Fig. 1 in (p, q) -space.

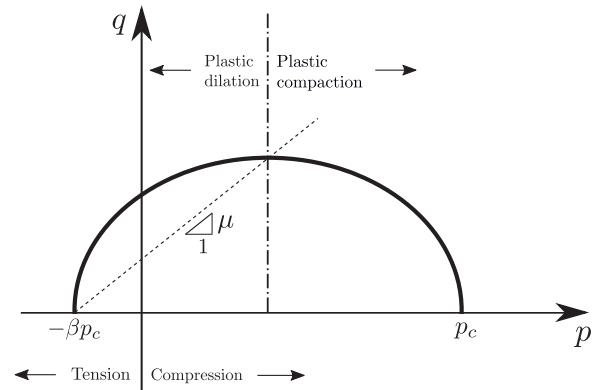


Figure 1. MCC yield surface described by p_c, β and μ .

An associated flow rule is adopted here, as is common in MCC models. Consequently, the plastic states will, unless at critical state, undergo either dilation or compaction as sketched in the above figure. The evolution of the yield surface with volumetric deformation (measured by the volumetric plastic Hencky strain ε_v^P) is controlled by a hardening law. Here, we consider such a law on p_c as

$$p_c(\varepsilon_v^P) = p_c^0 e^{-\xi \varepsilon_v^P} \quad (5)$$

where $p_c^0 \geq 0$ is an initial compressive strength and $\xi \geq 0$ is a dimensionless parameter. This hardening law can be motivated from the observed behavior of the slow compaction of soils, powders and brittle snow [18–20] as $1/\phi = 1/\phi^0 - \Lambda \ln(p_c/p_c^0)$ where $\Lambda > 0$ is called the plasticity index and ϕ^0 is the initial solid volume fraction. Assuming that the elastic deformation is negligible and that the total volumetric deformation is small, Eq. (5) is retrieved with $\xi = (\phi^0 \Lambda)^{-1}$.

Only at critical state will μ represent the factor of proportionality between the pressure p and equivalent shear stress q . Assuming that a flowing state should be described by the $\mu(I)$ -rheology [4, 5] and that the flowing state eventually aligns with critical state, we can make the CSL dependent on the inertial number, in particular,

$$\mu = \mu(I) = \mu_1 + \frac{\mu_2 - \mu_1}{\omega \sqrt{\bar{p}}/\dot{\gamma}_s + 1} \quad (6)$$

analogous to the form of [21], directly inserting for the inertial number $I = \dot{\gamma}_s d_* / \sqrt{\bar{p}}/\rho_*$ where ρ_* and d_* are the

Parameter	Symbol	Unit
Initial bulk density	ρ^0	kg/m ³
Young's modulus	E	Pa
Poisson's ratio	ν	-
Cohesion constant	β	-
Hardening constant	ξ	-
Initial compressive strength	p_c^0	Pa
Lower CSL	μ_1	-
Upper CSL	μ_2	-
Rheology constant	ω	kg ^{-1/2} m ^{1/2}

Table 1. Parameters of the MCC- $\mu(I)$ -rheology model.

intrinsic grain density and diameter, respectively. For convenience, the constant $\omega = I_0/(d_* \sqrt{\rho_*})$ is introduced. In Eq. (6), $\dot{\gamma}_s = \sqrt{2} \|\text{dev}(l^P)\|_F$ is the equivalent plastic shear strain rate. Moreover, $\bar{p} = p + \beta p_c$, i.e., we add the cohesive stress to the pressure in the definition of the inertial number, thus avoiding negative pressure, following the general ideas of [22, 23] where such a "cohesive" inertial number was proposed.

One interesting consequence of the elastoplastic nature of this model is that, due to the presence of its elastic regime, there is no need for partial regularization of the functional form of $\mu(I)$ for low inertial numbers. However, strain softening generally leads to ill-posedness, particularly in the inviscid limit, and common regularization techniques used in elastoplasticity may be needed depending on the purpose of the study.

5 Examples

Using the MCC- $\mu(I)$ -rheology model with cohesion parameter $\beta = 0.3$, a three-dimensional simulation of a cohesive granular cylinder is shown in Fig. 2. On the upper surface of the cylinder, crack patterns can be seen followed by the formation of cohesive blocks of material that persist during most of the collapse. These surface patterns are qualitatively reminiscent of the various patterns recently unveiled in the experimental campaign of [24]. Furthermore, on the side, shear bands are visible at the beginning of the collapse, oriented at an angle with each other.

Fig. 3 shows that the runout of a granular collapse decreases with increasing cohesion β . These collapse simulations were configured as in the experimental investigations by [25], using the same geometry and rheological parameters. Without trying to correlate the grain-grain attraction force measured in those experiments with the cohesion parameter β , the experimentally measured runout distances are included in Fig. 3 for comparison.

While cohesion is adjusted through β , the compressibility can be controlled through the hardening law, especially through the parameter ξ . In a granular collapse similar to the one described above, Figure 4 shows how the solid fraction evolves with changing ξ as well as the slope angle θ . Although Table 1 may give the impression of many model parameters, it may be helpful to consider that the elastic parameters will have little influence when the behavior is dominantly plastic.

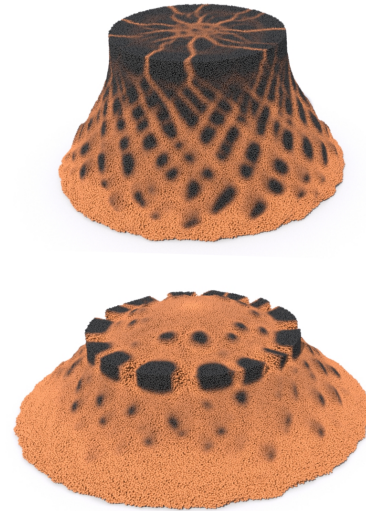


Figure 2. Cohesive collapse of cylinder (10 × 15 cm) at two different times (upper: $t = 0.14$ s, lower: $t = 0.19$ s) using the MCC- $\mu(I)$ -rheology model with $\beta = 0.3$. Increasingly orange colors represent increasing (plastic) shear strain rate.

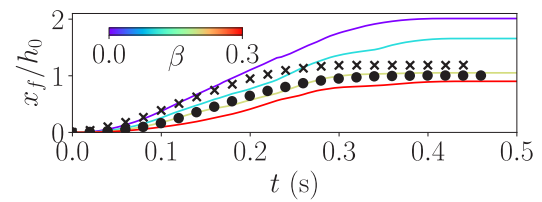


Figure 3. Cohesive collapse runout distance x_f (relative to initial height h_0) with increasing cohesion β compared to two experiments by [25] (circular and cross markers).

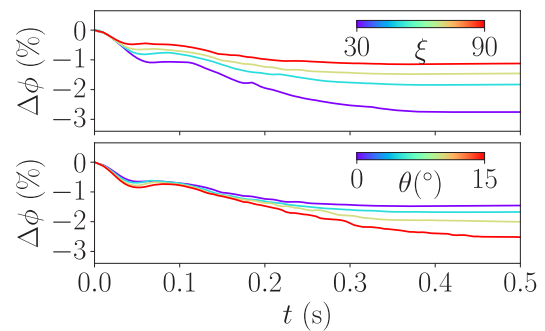


Figure 4. Change in solid volume fraction ϕ in granular collapse (with $\beta = 0$), changing hardening parameter ξ and slope angle θ .

As mentioned, MPM is capable not only of directly simulating the free surface, but can also naturally handle disconnections from the boundary. This is particularly relevant when simulating liftoff from terrains with bumps or cliffs, e.g., as often witnessed in avalanches and landslides. Complex terrains are easy to treat in MPM as they can simply be considered as level sets. In Fig. 5, a cohesive flow on a mountainous terrain is shown. In this case, a Coulomb frictional boundary condition is used where the Coulomb basal friction is set equal to the local value of μ of the flowing material [26]. The reader is referred to [1] for other examples of flow problems.

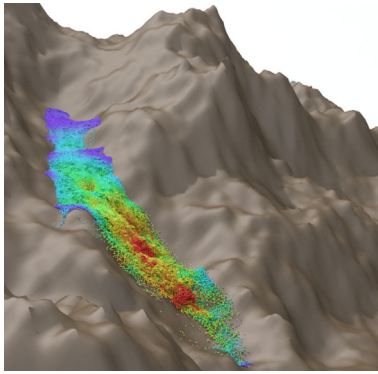


Figure 5. Avalanche on complex terrain.

6 Conclusion

In this short paper, we have discussed the use of elasto-viscoplastic models implemented in MPM to simulate granular media through both their solid and liquid phase. The MCC- $\mu(I)$ -rheology model was here the primary example, allowing us to account for both cohesion and compressibility in a single model that incorporates critical state behavior and the $\mu(I)$ -rheology. The granular gas phase and non-locality have not been considered, and in this context kinetic theory can provide a universal description of very dilute to dense granular flow [27]. In our models, compressibility is considered through a tunable hardening law, however, the $\phi(I)$ -rheology is not directly considered. Finally, the MPM numerical scheme enables a straightforward approach to future studies of, e.g., the process of erosion and the emergence of roll-waves.

The models presented in this paper are publicly available in the open-source MPM solver *Matter* [26, 28].

References

- [1] L. Blatny, J. Gray, J. Gaume, *J. Fluid Mech.* **997**, A67 (2024). [10.1017/jfm.2024.643](https://doi.org/10.1017/jfm.2024.643)
- [2] A.N. Schofield, P. Wroth, *Critical State Soil Mechanics* (McGraw-Hill London, 1968)
- [3] K.H. Roscoe, J.B. Burland, in *Engineering Plasticity* (CUP, Cambridge, UK, 1968), pp. 535–609
- [4] GDR MiDi, *The Eur. Phys. J. E* **14**, 341 (2004). [10.1140/epje/i2003-10153-0](https://doi.org/10.1140/epje/i2003-10153-0)
- [5] P. Jop, Y. Forterre, O. Pouliquen, *Nature* **441**, 727 (2006). [10.1038/nature04801](https://doi.org/10.1038/nature04801)
- [6] T. Barker, D.G. Schaeffer, M. Shearer, J.M.N.T. Gray, *Proc. R. Soc. A* **473**, 20160846 (2017). [10.1098/rspa.2016.0846](https://doi.org/10.1098/rspa.2016.0846)
- [7] D.G. Schaeffer, T. Barker, D. Tsuji, P. Gremaud, M. Shearer, J.M.N.T. Gray, *J. Fluid Mech.* **874**, 926 (2019). [10.1017/jfm.2019.476](https://doi.org/10.1017/jfm.2019.476)
- [8] Z. Wieckowski, S.K. Youn, J.H. Yeon, *Int. J. Numer. Methods Eng.* **45**, 1203 (1999). [10.1002/\(SICI\)1097-0207\(19990730\)45:9<1203::AID-NME626>3.0.CO;2-C](https://doi.org/10.1002/(SICI)1097-0207(19990730)45:9<1203::AID-NME626>3.0.CO;2-C)
- [9] S. Dunatunga, K. Kamrin, *J. Fluid Mech.* **779**, 483 (2015). [10.1017/jfm.2015.383](https://doi.org/10.1017/jfm.2015.383)
- [10] D. Sulsky, Z. Chen, H.L. Schreyer, *Comput. Methods Appl. Mech. Eng.* **118**, 179 (1994). [10.1016/0045-7825\(94\)90112-0](https://doi.org/10.1016/0045-7825(94)90112-0)
- [11] M. Steffen, R.M. Kirby, M. Berzins, *Int. J. Numer. Methods Eng.* **76**, 922 (2008). [10.1002/nme.2360](https://doi.org/10.1002/nme.2360)
- [12] C. Jiang, C. Schroeder, J. Teran, *J. Comput. Phys.* **338**, 137 (2017). [10.1016/j.jcp.2017.02.050](https://doi.org/10.1016/j.jcp.2017.02.050)
- [13] Y. Fei, Q. Guo, R. Wu, L. Huang, M. Gao, *ACM Trans. Graph.* **40**, 1 (2021). [10.1145/3450626.3459678](https://doi.org/10.1145/3450626.3459678)
- [14] H. Xiao, L.S. Chen, *Acta Mech.* **157**, 51 (2002). [10.1007/BF01182154](https://doi.org/10.1007/BF01182154)
- [15] P. Perzyna, *Quart. Appl. Math.* **20**, 321 (1963). [10.1090/qam/144536](https://doi.org/10.1090/qam/144536)
- [16] J.C. Simo, *Comput. Methods Appl. Mech. Eng.* **99**, 61 (1992). [10.1016/0045-7825\(92\)90123-2](https://doi.org/10.1016/0045-7825(92)90123-2)
- [17] J. Gaume, T. Gast, J. Teran, A. van Herwijnen, C. Jiang, *Nat. Commun.* **9**, 3047 (2018). [10.1038/s41467-018-05181-w](https://doi.org/10.1038/s41467-018-05181-w)
- [18] E.E. Walker, *Trans. Faraday Soc.* **19**, 73 (1923). [10.1039/TF9231900073](https://doi.org/10.1039/TF9231900073)
- [19] D.M. Wood, *Soil Behaviour and Critical State Soil Mechanics*, 1st edn. (CUP, 1991), ISBN 978-0-521-33249-1
- [20] L. Blatny, H. Löwe, J. Gaume, *Acta Mater.* **250**, 118861 (2023). [10.1016/j.actamat.2023.118861](https://doi.org/10.1016/j.actamat.2023.118861)
- [21] P. Jop, Y. Forterre, O. Pouliquen, *J. Fluid Mech.* **541**, 167 (2005). [10.1017/S0022112005005987](https://doi.org/10.1017/S0022112005005987)
- [22] N. Berger, E. Azéma, J.F. Douce, F. Radjai, *Europhys. Lett.* **112**, 64004 (2015). [10.1209/0295-5075/112/64004](https://doi.org/10.1209/0295-5075/112/64004)
- [23] T.T. Vo, S. Nezamabadi, P. Mutabaruka, J.Y. Delenne, F. Radjai, *Nat. Commun.* **11**, 1476 (2020). [10.1038/s41467-020-15263-3](https://doi.org/10.1038/s41467-020-15263-3)
- [24] R.S. Sharma, W. Sarlin, L. Xing, C. Morize, P. Gondret, A. Sauret, *Phys. Rev. Fluids* **9**, 074301 (2024). [10.1103/PhysRevFluids.9.074301](https://doi.org/10.1103/PhysRevFluids.9.074301)
- [25] A. Gans, A. Abramian, P.Y. Lagrée, M. Gong, A. Sauret, O. Pouliquen, M. Nicolas, *J. Fluid Mech.* **959**, A41 (2023). [10.1017/jfm.2023.180](https://doi.org/10.1017/jfm.2023.180)
- [26] L. Blatny, J. Gaume, *EGUsphere* **2025**, 1 (2025). [10.5194/egusphere-2025-1157](https://doi.org/10.5194/egusphere-2025-1157)
- [27] D. Berzi, *Phys. Rev. Fluids* **9**, 034304 (2024). [10.1103/PhysRevFluids.9.034304](https://doi.org/10.1103/PhysRevFluids.9.034304)
- [28] L. Blatny, J. Gaume, *Matter* (2025), Zenodo, GitHub, <https://github.com/larsblatny/matter>, [10.5281/ZENODO.15052338](https://doi.org/10.5281/ZENODO.15052338)